Inorganic Chemistry

Article

pubs.acs.org/IC

$Co_4(OH)_2(C_{10}H_{16}O_4)_3$ Metal–Organic Framework: Slow Magnetic Relaxation in the Ordered Phase of Magnetic Chains

Romain Sibille,* Thomas Mazet, Bernard Malaman, Thomas Gaudisson, and Michel François

Institut Jean Lamour, UMR 7198—Nancy Université, BP 70239, 54506 Vandoeuvre-lès-Nancy Cedex, France

Supporting Information

ABSTRACT: Reported here are the synthesis and structural and topological analysis as well as a magnetic investigation of the new $Co_4(OH)_2(C_{10}H_{16}O_4)_3$ metal–organic framework. The structural analysis reveals a one-dimensional inorganic subnetwork based on complex chains of cobalt(II) ions in two different oxygen environments. Long alkane dioic acid molecules bridge these inorganic chains together to afford large distances and poor magnetic media between dense spin chains. The thermal dependence of the χT product provides evidence for uncompensated antiferromagnetic interactions within the cobaltous chains. In zero-field, dynamic magnetic susceptibility measurements show slow magnetic relaxation below 5.4 K while both neutron diffraction and heat capacity measurements give evidence of long-range order (LRO) below this temperature. The slow dynamics may originate from the motion of broad domain walls and is characterized by an Arrhenius law with a single energy barrier $\Delta_\tau/k_B = 67(1)$ K for the [10–5000 Hz] frequency range. Moreover, in nonzero dc fields the ac susceptibility signal splits into a low-temperature frequency-dependent peak and a high-temperature frequency-independent peak which strongly shifts to higher temperature upon increasing the bias dc field. Heat capacity measurements have been carried out for various applied field values, and the recorded $C_P(T)$ data are used for the calculation of the thermal variations of both the adiabatic temperature change ΔT_{ad} and magnetic entropy change ΔS_m. The deduced data show a modest magnetocaloric effect at low temperature. Its maximum moves up to higher temperature upon increasing the field variation, in relation with the field-sensibility of the intrachain magnetic correlation length.

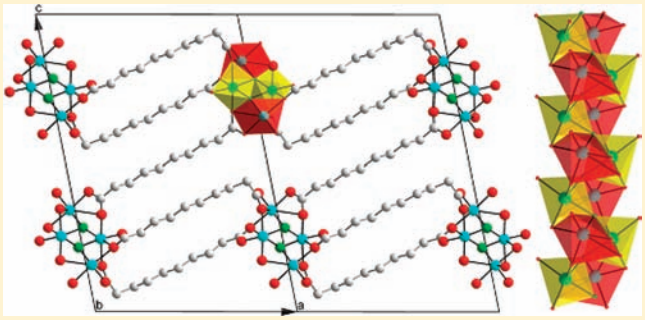

INTRODUCTION

The field of metal–organic framework (MOF) materials continues to expand at a remarkable pace,[1] in part because of the limitless number of possibilities, but also because of their ability to produce interesting properties for both industrial applications and fundamental science. By their unique structural and composition diversities, MOF materials are a huge source of experimental systems for exploring magnetism.[2,3] Magnetism of MOFs is increasingly studied as these materials can easily give 0D, 1D, or 2D inorganic (magnetic) subnetworks which are separated by adequately functionalized molecules. MOFs can be classified by using the simple notation I^mO^n where m and n represent the dimensionality of the inorganic and organic connectivity, respectively.[4] In magnetic MOFs, the organic moiety can either act as a simple spacer between spin clusters, chains, or layers, or as an active component of the whole material. In the former case, magnetically inert molecules such as alkane chains can be used for tuning distances between spin systems.[5,6] In the latter case, it can lead up to the juxtaposition of different properties in the same material or to new properties by a synergic interplay between the organic and inorganic subnetworks. The majority of magnetic MOFs are those containing paramagnetic metal centers like 3d and 4f elements although some compounds are also based on stable radicals. Among these paramagnetic metallic centers, cobalt holds an important place[3] and has given a wide variety of original magnetic phenomena owing to its anisotropic spin and its ability to bind with various ligands in many coordination modes.

One-dimensional magnetic systems are of great interest in physics since the theoretical models are more tractable than the same models developed at higher dimensions. Since the pioneering work of R.J. Glauber in 1963,[7] it was predicted that slow magnetic dynamics can be obtained by considering chains combining a large magnetic anisotropy and ferromagnetic interactions. The first experimental observation was only reported in 2001 in the $[Co^{II}(hfac)_2 \cdot NITPhOMe]$ polymer where hfac = hexafluoroacetylacetonate and NITPhOMe = 4′-methoxy-phenyl-4,4,5,5,-tetramethylimidazoline-1-oxyl-3-oxide.[8] It has been shown that the measured slow relaxation of the magnetization and hysteresis effects are not associated with long-range order (LRO) in this compound. Since this breakthrough, a relatively small number of similar examples have been reported, either MOFs or metallosupramolecular assemblies. The term single-chain magnet (SCM) has since been adopted for this new class of magnets. SCM materials are thus composed of magnetically

Received: September 27, 2011
Published: February 17, 2012

dx.doi.org/10.1021/ic2020995 | Inorg. Chem. 2012, 51, 2885–2892

isolated chains for which a finite magnetization can be frozen in the absence of an applied magnetic field. In 2009 it has been theoretically demonstrated[9] as well as experimentally observed[9,10] that SCM behavior can still occur in an antiferromagnetically ordered phase of spin chains. The considered compounds were made of $Mn^{III}_2Ni^{II}$ units, and their applied field versus temperature phase diagrams exhibit the characteristic paramagnetic−antiferromagnetic line of metamagnetic materials. In these materials, a Néel transition appears first and the SCM slow dynamics is observed at lower temperature. Also of interest is a recent report of a 2D metamagnetic compound composed of ferromagnetic Co^{II} chains exhibiting the slow relaxation of SCMs either in the antiferromagnetic ordered phase or in the field-induced ferromagnetic phase.[11]

Quite generally, it was hitherto believed that LRO did prevent the intrinsic slow dynamics of the spin chains. However, the observation of slow relaxation of the magnetization in ordered phases of ferrimagnetic chains was reported as far back as 2002.[12] The considered compounds were complexes of general formula $[M^{II}(hfac)_2{\cdot}radical]$ where M = Co or Mn and radical = methyl[3-(4,4,5,5-tetramethyl-4,5-dihydro-1*H*-imidazolyl-1-oxy-3-oxide)phenoxy]-2-propionate, namely 3MLNN;[12] 5-*R*-1,3-bis(*N*-tert-butyl-*N*-oxylamino)benzene (R = H, F, Cl, Br), namely BNO_R;[13] or *para*-butoxyphenyl-(4,4,5,5-tetramethyl-4,5-dihydro-1*H*-imidazolyl-1-oxy-3-oxide), namely BPNN.[14] In these compounds, slow dynamics can either occur at the LRO transition temperature or at lower temperature, depending on the nature of both the 3d-metal spin and the organic spin. A quantum dissipation theory of slow magnetic relaxation mediated by domain-wall motion has been reported for the compound based on Mn^{II} and BNO_H radicals.[15] The complex based on Co^{II} and BPNN radicals was reported in 2008.[14] The authors found an LRO at a quite large temperature of 45 K and a SCM-like behavior around 10 K. This material has an unusually large coercive field of 5.2 T that might be related to the intrinsic properties of the chains.[16]

As part of our ongoing research on new magnetic metal−organic frameworks based on dicarboxylic molecules and 3d metal−hydroxide layers, we are currently working with simple alkane dioic acid linkers of various lengths in order to tune distances between spin layers in isoreticular crystalline frameworks $(M^{II}_5(OH)_6(C_nH_{2n-4}O_4)_2$, n = 6, 8, 10...).[6] These linkers are interesting because they combine σ-bonded alkyl chains which are poor magnetic media with the ability to bind on both sides with cations. By the use of a two-step procedure allowing fine control of the pH during the synthesis, we obtained a purple crystalline material of formula $Co_4(OH)_2(C_{10}H_{16}O_4)_3$ (noted I^1O^2-CoC_{10}) instead of the attempted pink I^2O^1 $Co_5(OH)_6(C_{10}H_{16}O_4)_2$ material. In the first part of this Article, we describe the synthesis, structure, and topology of this new MOF. Our contribution then focuses on a detailed investigation of the magnetism of this compound. In particular we show that I^1O^2-CoC_{10} displays slow dynamics of the magnetization in its quasi-1D structure of magnetically ordered chains. This behavior was previously observed in some of the $M^{II}(hfac)_2$−nitronyl nitroxide compounds cited above within which the spins arise from the presence of both 3d metallic elements and organic radicals. We report a similar behavior in a compound based only on the anisotropic spin of Co^{II} ions. The evidence of the LRO is given by neutron diffraction and heat capacity (C_P) measurements. $C_P(T)$ data are also used for the calculation of the magnetocaloric properties.

EXPERIMENTAL SECTION

Synthesis. All chemicals were commercially available from Aldrich and used as received. I^1O^2-CoC_{10} was synthesized according to the following procedure: sebacic acid (6 mmol, 1.22 g) was dissolved into 10 mL of distillated water. The pH of the starting solution was finely adjusted by NaOH droplets to 8.0. The resulting solution was placed into a homemade 50 mL plastic reactor under constant argon current to avoid the formation of cobalt oxide impurities. This hermetic reactor was equipped with two injectors, a pH electrode, and magnetic stirring. The system was deoxygenated for 10 min before the combined addition of the $CoCl_2{\cdot}6H_2O$ (3 mmol, 0.72 g in 10 mL of water) and NaOH (≈20 mmol, 40 mL 0.5 M) solutions by the two injectors. The addition was driven by two peristaltic pumps (Ismatec) and the electrode was linked to a pH-meter (Knick). The two peristaltic pumps and the pH-meter were driven by a computer via the Labworldsoft program. The addition of the metallic salt solution was done at a constant rate while the addition rate of the basic solution was varied in order to keep a constant pH value during the whole course of the addition (4 h). After this first step, the mixture was stirred for five more minutes and then sucked up by a syringe which was then transferred into a glovebox under argon atmosphere. The mixture was finally transferred into a Teflon-walled stainless steel autoclave under the argon atmosphere. Following this first step, the titled compound was obtained by a hydrothermal treatment between 150 and 180 °C. After three days, the autoclave was naturally cooled in air and opened under ambient atmosphere. Small microcrystals (see photograph in Supporting Information) were isolated for X-ray crystallography. The powdered reaction product used for all the other characterizations was collected by centrifugation, washed twice with a mixture of distilled water and ethanol (1/1), and then dried at room temperature. Yield (based on cobalt): 83%.

The first step of our procedure was important for two different aspects of the synthesis. On one hand, the controlled regulation with the peristaltic pumps allows a very small pH variation during the whole course of the mixing (typically between 7.95 and 8.05). This first point was crucial for the synthesis of our material as a pure phase. On the other hand, we think that the good crystallinity of the resulting material has to be related to the slow mixing of the reactants together. Finally, it is noticeable that a similar synthesis using all the reactants mixed in one pot does not lead to the formation of the considered framework. At the present time, it remains difficult to know if the very slow mixing of the reactants is a necessary condition for the synthesis of this compound or if its formation is allowed by the fine pH regulation. A careful and detailed investigation of the synthesis is required in order to fully understand the kinetic and thermodynamic conditions leading to the formation of this new framework. Nevertheless, powders of I^1O^2-CoC_{10} as well as a few microcrystals suitable for single-crystal X-ray diffraction analysis were repeatedly obtained by using this procedure.

Physical Measurements. Thermogravimetric measurement was performed using a Setaram TGDTA-92 thermobalance. Samples were placed in alumina containers, and data were recorded in air between 20 and 600 °C, with a heating rate of 1 °C/min. The data were corrected for the empty container. An FTIR spectrum was obtained with a Bruker Vertex 80v spectrometer in the region 500−4000 cm^{-1}. Samples were prepared as disks of dried KBr (100 mg) mixed with a small amount of the sample (3 mg). A dried KBr disk was used as baseline correction. Powder X-ray diffraction data were collected at room temperature using filtered Cu Kα radiation (λ = 1.5418 Å) and a reflection θ−θ geometry (Philips X-Pert Pro diffractometer). Single crystal X-ray diffraction data were collected with an Oxford Supernova diffractometer equipped with a Mo Kα radiation microsource and an Atlas CCD detector. Direct current and alternating current magnetic susceptibility measurements were carried out with a PPMS-9T Quantum Design magnetometer between 2 and 300 K. Alternating current susceptibility measurements were recorded using an alternative magnetic field μ_0H_{AC} = 0.5 mT either with or without bias dc field. The 10 mg polycrystalline specimen was encapsulated into a gelatin sample holder. The magnetic response was corrected with diamagnetic

dx.doi.org/10.1021/ic2020995 | *Inorg. Chem.* 2012, 51, 2885−2892

blank data of the sample holder obtained separately, and the diamagnetic contribution of the sample itself was estimated from Pascal's constants. Heat capacity measurements were also recorded with the PPMS-9T Quantum Design apparatus equipped with the heat capacity module as well as with a cryopump that allows working under secondary vacuum. Data were obtained in the temperature range [2.5−50 K] under various dc fields. The addenda were first recorded for the heat capacity platform and for the grease (Apiezon N) which was used to fix the 10 mg polycrystalline sample on the heat capacity platform. In these conditions, the sample contribution to the total heat capacity signal was 4 (50 K) to 32 (2.5 K) times larger than the addenda contribution. Powder neutron diffraction experiments were carried out at the Institut Laue Langevin, Grenoble (France), using the D1B two-axis diffractometer (λ = 2.52 Å, step of 0.2° 2θ). The neutron diffraction patterns were recorded in the paramagnetic state (15 K) and in the ordered magnetic state (1.5 K) using a standard helium cryostat. Owing to the large incoherent neutron scattering length of hydrogen atoms (100 H atoms per unit cell), such neutron diffraction experiments are very time-consuming. The patterns recorded at 15 and 1.5 K were 10 h each.

Sample Homogeneity. The homogeneity of the sample used for the physical measurements was checked by powder X-ray diffraction (PXRD), thermogravimetric analysis (TGA), and chemical analysis (Anal. (Calcd): C, 40.87 (41.39); O, 25.31 (25.76); Co, 27.48 (27.10)). Starting from the single-crystal structure of I^1O^2-CoC_{10} (see below for details), the obtained powder pattern was analyzed by the Lebail method using the FOX software.[17] The final plot of this whole-pattern decomposition is available as Supporting Information. Agreement factors converge satisfactorily to values lower than 3%. The TGA trace (see Supporting Information) shows decomposition in air above 220 °C. The weight loss occurs in a single broad step up to 380 °C which is related to the degradation of the sebacate molecules (−59.76% observed; −63.07% calculated for the reaction 1 $Co_4(OH)_2(C_{10}H_{16}O_4)_3$ gives $^4/_3$ Co_3O_4). The purity of the Co_3O_4 residue was checked by PXRD.

FTIR. Fourier transform infrared spectrum of I^1O^2-CoC_{10} is available in Supporting Information. It clearly shows the stretching vibrations of OH^-, COO^-, and alkyl CH groups. A sharp band at 3448 cm^{-1} is assigned to the stretching vibration of OH groups not involved in hydrogen bonding. Characteristic alkyl CH stretching bands are found at 2975, 2962, 2954, 2937, 2925, 2893, 2863, and 2852 cm^{-1}. Two intense bands at 1554 and 1398 cm^{-1} are assigned to $\nu_{as}(COO^-)$ and $\nu_s(COO^-)$, respectively. Such a small splitting ($\Delta\nu_{as\text{-}s}$ = 156 cm^{-1}) between the carboxylate stretching frequencies is characteristic of bridging carboxylates in accordance with the crystallographic structure of the compound (see below).

Single-Crystal X-ray Diffraction. A single crystal (50 μm × 20 μm × 10 μm) was mounted on the end of a glue fiber and placed in a nitrogen cold stream at 100(2) K. A total of 20 974 reflections (2841 independent) were collected, integrated, and scaled using CrysAlisPro, Oxford Diffraction Ltd., Version 1.171.33.55. The frames were collected by ω-scans, and absorption corrections were done using the multiscan method (μ = 2.016 mm^{-1}). The frames were collected up to 2θ = 49.42°. Co, C, and O atoms were located by direct methods with the SIR92 software,[18] and the model refinement was carried out using all reflections and full matrix least-squares on F^2 with SHEXLTL.[19] All non-hydrogen atoms were refined anisotropically. Hydrogen atoms were added using geometrical constraints (HFIX command). The refinement procedure includes 218 parameters and converges satisfactory down to R1 = 0.0545 for the 1700 reflections with $I > 2\sigma_I$ and R1 = 0.1063 for the 2841 reflections.

RESULTS AND DISCUSSION

Crystal Structure. The I^1O^2-CoC_{10} MOF crystallizes in the monoclinic $P2_1/c$ space group (see Table 1 and Figure 1). We first consider the cobalt chains running along the *b*-axis that constitute the inorganic subnetwork (Figure 2). These chains are made of two independent cobalt sites in general position, each site giving a pair of two positions (noted a and b) related by the 2-fold screw axis. The Co1 atom is coordinated in a slightly distorted octahedral CoO_6 geometry to two OH^- groups and four carboxylate O atoms coming from four sebacate ligands. Co1 atoms are linked together by the OH^- group to form [Co1a−OH−Co1b] infinite zigzag chains with an angle of 136° and Co1a−Co1b distances of 3.857(2) Å. The Co2 atom coordinates in trigonal bipyramidal CoO_5 geometry with one OH^- group and four O atoms from four distinct molecules. A sixth O atom is more distant from Co2. Co2a and Co2b atoms do not share any O atom, but each Co2 atom shares four O atoms with three Co1 atoms. In particular, one comes from the OH^- group linking the Co1 atoms together and thus acting as a μ_3-OH group

Table 1. Selected Crystallographic Parameters and Interatomic Distances for I^1O^2-CoC_{10}

Crystallographic Parameters					
formula		$Co_4(OH)_2(C_{10}H_{16}O_4)_3$			
MW		870.42 g mol^{-1}			
Z		4			
space group		$P2_1/c$			
a		15.1992(14) Å			
b		4.9120(4) Å			
c		22.877(2) Å			
β		101.504(10)°			
V		1673.6(3) $Å^3$			
ρ_{calcd}		1.727 g cm^{-3}			
Interatomic Distances (Å)					
Co1	O_{OH}	2.083(7)	Co2	O_{OH}	2.024(7)
	O_{OH}	2.076(7)		O_{COO} 1	2.022(4)
	O_{COO} 1	2.203(5)		O_{COO} 2	2.137(13)
	O_{COO} 2	2.128(5)		O_{COO} 3	2.745(6)
	O_{COO} 3	2.130(6)		O_{COO} 5	2.025(12)
	O_{COO} 4	2.062(5)		O_{COO} 6	2.011(7)

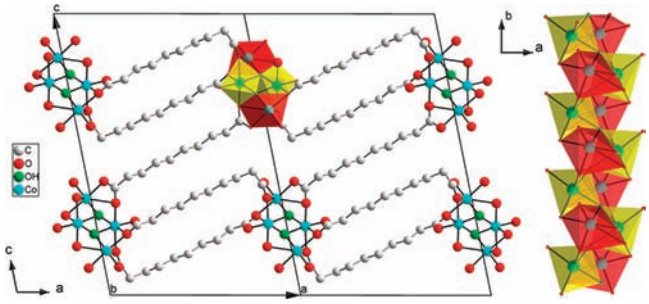

Figure 1. Structure of I^1O^2-CoC_{10}. Left: View along the *b*-axis showing the connectivity between the inorganic chains in the framework. Right: Metallic sites in the inorganic chains (yellow, Co1; red, Co2). Hydrogen atoms have been omitted for clarity.

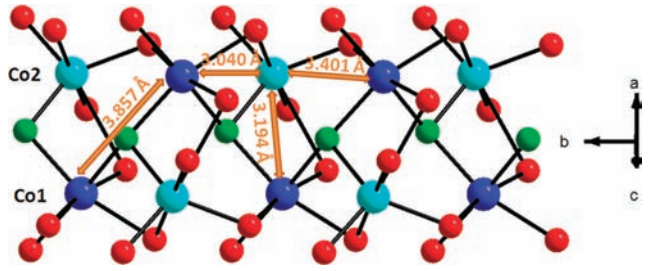

Figure 2. Structure of the inorganic chains in I^1O^2-CoC_{10}. Oxygen: red (carboxylate), green (hydroxyl). Cobalt: blue (Co1), cyan (Co2). Hydrogen atoms have been omitted.

dx.doi.org/10.1021/ic2020995 | Inorg. Chem. 2012, 51, 2885−2892

in the inorganic chains. To put emphasis on the magnetic superexchange pathways, a Co2 atom is linked to three Co1 atoms by (i) a single Co−O−Co pathway (Co···Co = 3.401(6) Å) with an angle of about 107.1°, (ii) two Co−O−Co pathways (Co···Co = 3.194(1) Å) with angles of 102.4° and 80.8°, (iii) two Co−O−Co pathways (Co···Co = 3.040(7) Å) with angles of 90.9° and 95.5°. The inorganic chains described so far are bridged by the means of two independent sebacate molecules. On the first hand, the sebacate-1 molecule adopts a hexadentate symmetric bridging mode and links the cobalt chains in the [100] direction. In this direction, adjacent inorganic chains are interlinked by two of these molecules to give infinite layers. This dicarboxylate also displays a large torsion angle of about 63° at one end of the alkyl chain. On the other hand, the sebacate-2 molecule bridges the inorganic chains in the [201] direction in a hexadentate symmetric bridging mode. This molecule gives its 3D character to the whole framework. Finally, the complete formula of the I^1O^2-CoC_{10} MOF is $Co_4(\mu_3\text{-}OH)_2[(\kappa^1\text{-}\kappa^1\text{-}\mu_2)\text{-}(\kappa^1\text{-}\kappa^1\text{-}\mu_2)\text{-}\mu_6\text{-}C_{10}H_{16}O_4]_2[(\kappa^2\text{-}\kappa^1\text{-}\mu_2)\text{-}(\kappa^2\text{-}\kappa^1\text{-}\mu_2)\text{-}\mu_4\text{-}C_{10}H_{16}O_4]$. The interchain distances of interest for the magnetic study are of three types: 15.20 Å in the [100] direction with two sebacate-1 molecules, 20.77 Å in the [201] direction with one sebacate-2 molecule, and 11.44 Å in the [001] direction without any chemical connection. These interchain distances are similar to that found in other systems exhibiting significant dipolar interactions.[20]

Topological Analysis. The framework can be simplified by the application of a topological approach (Figure 3).[21] Pairs

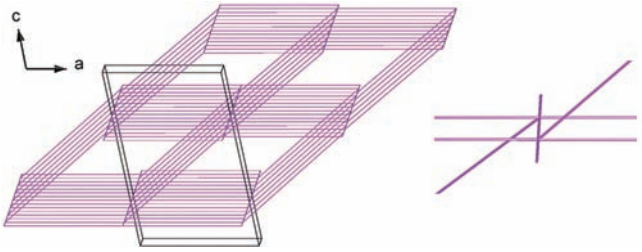

Figure 3. Topological representation of I^1O^2-CoC_{10}. Left: View of the bnn net compared with the crystallographic unit cell. Right: View of two adjacent trigonal bipyramidal nodes in the [010] direction.

of Co1−Co2 atoms have been considered as five-connected trigonal bipyramidal nodes. Two of these five connections link the nodes together in the [010] direction to describe the infinite inorganic chains. The three remaining connection are used for the connection of the inorganic chains together and via the alkane dioic acid molecules. Two of them are in the [100] direction via the sebacate-1 molecule, and the last one is in the [201] direction via the sebacate-2 molecule. The resulting framework is a bnn net of vertex symbol 4.4.4.4.4.4.6.6.6.*.

Direct Current Magnetic Measurements. The thermal dependence of the static susceptibility χ_{DC} has been recorded for an applied magnetic field $\mu_0 H_{DC}$ of 0.2 T. The data in the range 25−300 K obey the Curie−Weiss law $\chi = C/(T - \theta)$ with C = 2.33 cm^3 K mol^{-1} and θ = −8.6 K indicating intrachain antiferromagnetic interactions and/or spin−orbital coupling effects (see Supporting Information). The thermal variation of the χT product is represented in Figure 4a,b. At room temperature the χT value is 2.25 cm^3 K mol^{-1} per Co^{II} ion which is significantly larger than the $S = {}^3/_2$ spin-only value of 1.88 cm^3 K mol^{-1}, hence indicating an orbital contribution.[22] As it is

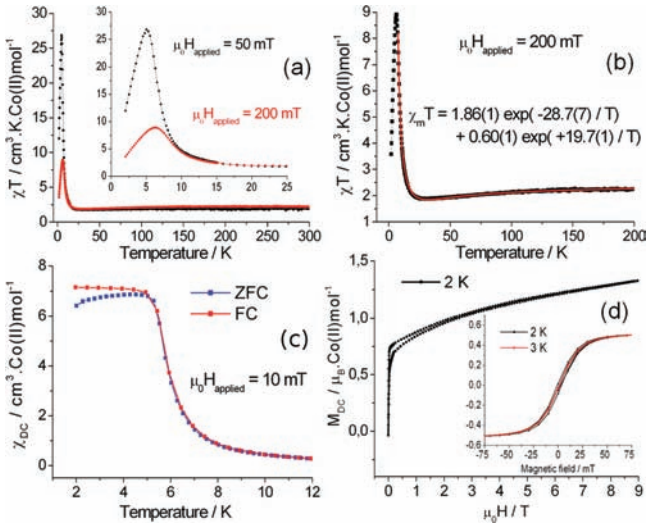

Figure 4. Direct current magnetic measurements. Plot of χT vs T for $\mu_0 H_{dc}$ = 50 and 200 mT (a) and its fit to the above equation (b). χ_{DC} vs T measured by zero-field-cooled (ZFC) and field-cooled (FC) methods for $\mu_0 H_{dc}$ = 10 mT (c). Magnetization vs field at low temperatures (d).

cooled down, the χT product decreases with decreasing temperature down to a minimum value of 1.88 cm^3 K Co^{II} mol^{-1} at 30 K. Below this temperature, the χT product shows a brutal increase to reach a maximum of 8.9 cm^3 K Co^{II} mol^{-1} around 6 K. The high temperature behavior is expected for ferrimagnetic chains and/or compounds containing orbitally degenerated ions whereas the low-temperature upsurge indicates ferrimagnetism or spin-canting. Upon consideration of both the numerous magnetic exchange pathways present within the inorganic chains and the two very different coordinating environments of the anisotropic Co^{II} spins, the presence of spin-canting, i.e., a noncollinear spin structure and/or different magnetic moment values for Co1 and Co2, is probable. Moreover, if we consider that the magnetocrystalline anisotropy of a cobalt site (for example Co2, see Figure 5) sets its magnetic

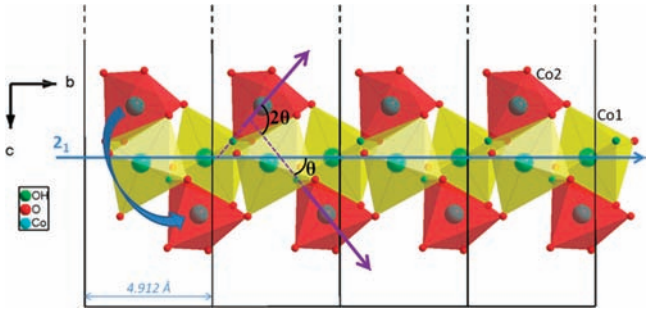

Figure 5. View of the magnetic chain along the *a*-axis. The horizontal blue arrow represents the 2-fold screw axis (2_1; 0, y, $^1/_4$), and the curved blue arrow shows the effect of this symmetry element on the position of a Co2 atom. The purple arrows on the Co2 sites represent an arbitrary anisotropy axis (making a nonzero θ angle with the *b*-axis) and the effect of the 2_1 symmetry element on its orientation.

moment into an orientation (for example the arbitrary orientation used in Figure 5) which is not collinear with the 2-fold screw axis, then this later necessarily implies a canting angle between the orientations of the anisotropy easy axes of the two Co2 positions generated by this symmetry element.

dx.doi.org/10.1021/ic2020995 | Inorg. Chem. 2012, 51, 2885−2892

A spin Hamiltonian description of the intrachain exchange interactions without any a priori assumptions is not straightforward for such complex magnetic chains. To get round this difficulty we chose to employ a recently developed "noncritical scaling" theory[23] which has shown that the minimum present in the thermal variation of the χT product is well described by the sum of two exponential functions $\chi T = C_1 \exp(E_1/T) + C_2 \exp(E_2/T)$ where $C_1 + C_2$ is the high temperature extrapolated Curie constant. The fit of the magnetic susceptibility of I^1O^2-CoC_{10} to this equation between 300 and 7 K (Figure 4b) yields $C_1 = 1.86(1)$ cm K Co^{II} mol^{-1}, $E_1 = -28.7(7)$ K, and $C_2 = 0.60(1)$ cm^3 K Co^{II} mol^{-1}, $E_2 = 19.7(1)$ K. The extrapolated Curie constant $C_1 + C_2 = 2.46$ cm^3 K Co^{II} mol^{-1} is in agreement with the value obtained by the Curie–Weiss fit. Here, the first term is a high-temperature antiferromagnetic contribution which represents the dominant intrachain interactions and spin–orbit effects, whereas the second term is a low-temperature ferromagnetic contribution that corresponds to the increase in the intrachain correlation length as described in the Ising model with, however, reduced effective spins because of partial compensation of the magnetic moments.[24] Figure 4c shows the low temperature thermal variation of the magnetic susceptibility. Upon cooling down, it increases suddenly around 5 K and then reaches a plateau down to 2 K. The zero-field-cooled (ZFC) and field-cooled (FC) measurements recorded under a field of 10 mT diverge below 5.4 K.

An uncompensated magnetic ground state is further supposed by the low temperature $M(H)$ plot (Figure 4d) which shows a sudden jump at very small external fields (i.e., less than 50 mT). The small value of the magnetization after this jump (≈0.6 μ_B per Co^{II} ion) confirms the presence of dominant antiferromagnetic interactions which are uncompensated by canting angles and/or different magnetic moments for Co1 and Co2. In addition, we observe hysteresis in the high-field region of the $M(H)$ plot which is likely to be related to single-ion anisotropy. The presence of a significant curvature in this high-field region, i.e., of an imperfect linear increase after the low-field jump, is comprehensible for a powdered sample with magnetic anisotropy.[24] Finally, the low-field isothermal magnetization curves at 2 and 3 K (inset of Figure 4d) show that the cycle starts to open very slightly with a coercive field of 5 mT at 2 K.

Evidence for LRO. Heat capacity measurements in the (2.5–50 K) temperature range have been carried out in order to get more insight about the dimensionality of the magnetism of I^1O^2-CoC_{10}. The $C_P(T)$ curve recorded under zero-field (Figure 6a) shows two anomalies, a λ-type peak at $T_t = 5.4$ K superimposed to a broad hump with maximum around 7 K. The peak at 5.4 K provides clear evidence of the realization of a 3D LRO state; its reduced height is due to the weak interchain couplings.[25] We attribute the rounded anomaly to short-range order (SRO) within the chains.[26] Upon field increase, the λ-peak smears out while the broad bump strongly shifts to higher temperature.

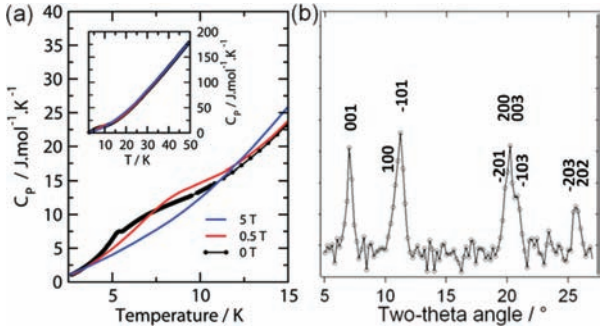

Figure 6. Long-range order in I^1O^2-CoC_{10}. (a) $C_P(T)$ data recorded in external dc fields of 0, 0.5, and 5 T. (b) Neutron diffraction difference pattern between 1.5 and 15 K, $\lambda = 2.52$ Å.

A preliminary neutron diffraction experiment has been performed and gives supplementary unambiguous proof of the LRO. The difference between patterns recorded at 15 and 1.5 K (Figure 6b) clearly shows the occurrence of additional peaks ($h0l$ with $l = 2n + 1$) forbidden by the $P2_1/c$ space group, thus indicating a magnetic anti c glide yielding dominant interchain antiferromagnetic coupling in the [001] direction. A careful analysis of the width of these peaks reveals weak ferromagnetic contributions at some nuclear Bragg positions (100, 200, 202), in accordance with a canted arrangement of the magnetic moments.

Alternating Current Magnetic Measurements. Dynamic ac magnetization measurements with frequencies ν in the 10–10 000 Hz range have been performed in order to clarify the nature of the magnetic state. The thermal variation of the complex ac susceptibility shows rounded peaks for both the real and imaginary parts. This first observation is in accordance with the existence of a ferromagnetic contribution. For a nil bias dc field (Figure 7a), both in-phase and out-of-phase components show strong frequency-dependent behavior. Below $T_t = 5.4$ K, M' and M'' shift to lower temperatures for lower frequencies which is expected for a SCM: as the temperature is lowered, correlations along the chain grow, and it becomes more difficult for the spins to follow the field.[27]

To clarify the nature of this relaxation process, a quantitative measure of the frequency dependence ($\Phi = (\Delta T_f/T_0)/\Delta(\log \nu)$)[28] can be used to distinguish glassiness and other phenomena such as superparamagnetism, domain-wall motion, and SCM behavior (T_f being the M'' maxima). The quite large Φ value obtained (0.22) tends to preclude the existence of spin-glass behavior arising from frustration. Moreover, Cole–Cole diagrams of χ'' versus χ' at various temperatures are represented in Figure 8a. They show imperfect semicircle shapes and can be fitted by the generalized Debye model[29] expression $\chi'' = (\chi_S - \chi_T) \tanh[\alpha\pi/2]/2 + \{(\chi' - \chi_S)(\chi_T - \chi') + (\chi_T - \chi_S)^2 \tanh^2[\alpha\pi/2]/4\}^{1/2}$. The obtained α values of 0.40–0.60 suggest a quite large distribution of relaxation processes. Such a distribution tends to exclude the single-spin process of SCMs for the magnetization dynamics of I^1O^2-CoC_{10}.

The energy barrier of the magnetization reorientation Δ_τ follows a thermally activated regime which can be modeled by an Arrhenius law, $\tau = \tau_0 \exp(\Delta_\tau/k_BT)$, where $\tau^{-1} = 2\pi\nu$ at the maxima of the $M''(T)$ curves and τ_0 is a pre-exponential factor. The best fit gives $\tau_0 = 1.4 \times 10^{-11}$ s and $\Delta_\tau/k_B = 67(1)$ K (Figure 8b), which are normal values for 1D systems such as SCMs or compounds with movement of broader domain walls. It is noteworthy that the higher temperature points of the Arrhenius plot are excluded because they significantly deviate from the linear fit. Spin–orbit coupling effects known for Co^{II} ions could be responsible for this slope change. In addition, dynamic magnetic measurements were also performed on microcrystals of I^1O^2-CoC_{10}, and the deduced Arrhenius plot was similar to that obtained for the powdered sample used during this study. In other words, it should indicate that the slope change in the Arrhenius plot is independent of the defects (dilution), namely, that it does not refer to finite-size effects.

dx.doi.org/10.1021/ic2020995 | Inorg. Chem. 2012, 51, 2885–2892

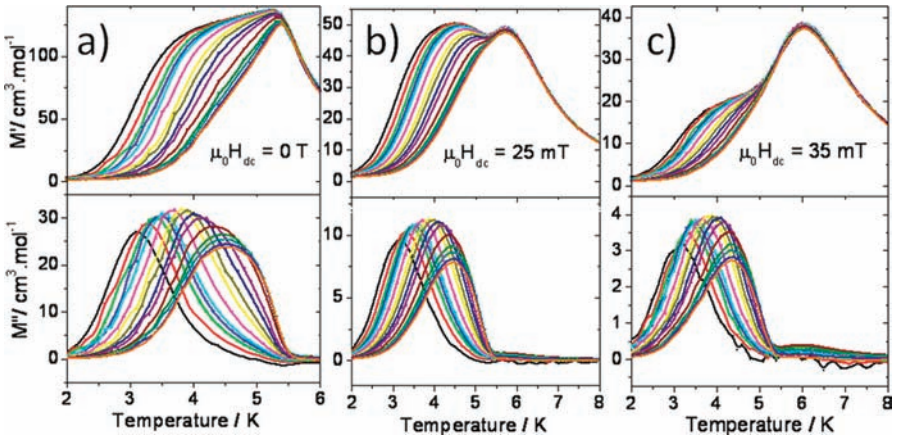

Figure 7. Alternating current magnetic measurements. Plot of M' (top) and M'' (bottom) vs T for μ_0H_{dc} = 0 (a), 25 (b), and 35 mT (c) (μ_0H_{ac} = 0.3 mT) for various frequencies from 10 (black curves) to 10 000 Hz (orange curves).

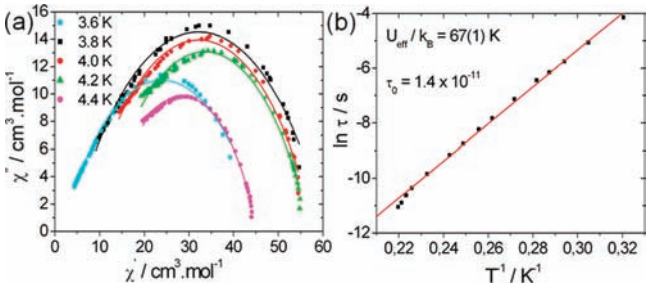

Figure 8. Analysis of ac magnetic measurements. (a) Cole−Cole plots at various temperatures for 1^1O^2-CoC_{10}. The solid lines represent the least-squares fit using a generalized Debye model. (b) Arrhenius plot obtained from the χ'' maxima recorded for μ_0H_{DC} = 0 T. The points at the highest frequencies (namely 6500, 8500, and 10 000 Hz) have been excluded of the fit (see text).

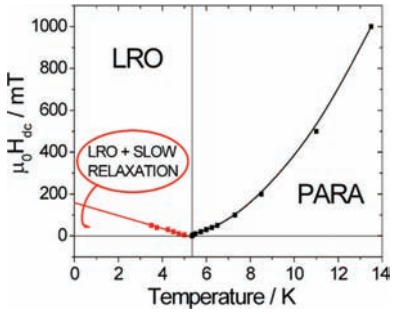

Figure 9. Plot of the ac susceptibility maxima under various dc fields. Red and black symbols correspond to the maxima of the frequency dependent ac signal and frequency-independent ac signal, respectively.

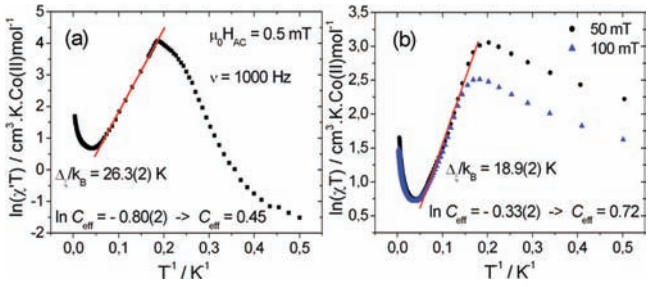

Figure 10. Logarithmic representation of χT vs T^{-1} from ac 100 Hz (a) and dc (b) data. The red lines represent the least-squares fit to the equation $\ln(\chi T) = \ln C_{eff} + \Delta_\xi/k_B \times T^{-1}$.

Alternating current magnetic measurements have also been carried out for various bias dc fields (Figure 7b,c and Supporting Information). The first clear result is that, for external fields lower than 100 mT, the ac signal splits into a low-temperature frequency-dependent peak and a high-temperature frequency-independent peak. The frequency dependence of the low-temperature signal has been analyzed for μ_0H_{dc} = 25 and 35 mT, and almost similar values of Δ_τ/k_B and τ_0 are found (see Supporting Information). The position of this low-temperature signal varies slightly toward lower temperature upon increasing the bias dc field, while its amplitude vanishes progressively. For the high-temperature signal, both the real part and the low-magnitude imaginary part of the ac susceptibility strongly shift to higher temperature upon increasing the bias dc field. The behavior of the ac susceptibility signal as a function of the dc field is summarized in Figure 9. The ac signal splitting observed in moderate bias fields is found to be in accordance with calculations based on the spin Hamiltonian for a randomly diluted ferrimagnetic chain in field.[30,31] In this theoretical approach, a "bulk" contribution which corresponds to an infinite 1D Ising system (zero dilution) shifts toward higher temperatures when the field increases because of the strong field effects on ξ.

As seen in the dc measurements, the thermal dependence of the magnetic susceptibility is exponential, as expected for a 1D Ising-like system,[27] and the plot of $\ln(\chi'T)$ versus $1/T$ in zero-field (Figure 10a) can be made to extract the energy barrier Δ_ξ/k_B of creating domain walls. By linearly fitting the expression $\chi'T = C_{eff}\exp(\Delta_\xi/k_BT)$ above T_t, we get Δ_ξ/k_B = 26.3(2) K. Assuming $\xi > L$, L being the chain length, i.e., the distance between two defects, the anisotropic barrier for the reversing of the magnetization of one spin can be deduced by the expression $\Delta_A/k_B = (\Delta_\tau - \Delta_\xi)/k_B$ (≈40 K). In the case of 1^1O^2-CoC_{10}, the relaxation process should significantly differ from the idealized single-spin process, and we must remain cautious with the use of this expression. However, it is noticeable that this value of the anisotropic barrier is of the order of magnitude of the exchange constants deduced by the noncritical scaling analysis. As the thickness of domain walls is controlled by the relative strength of the exchange and magnetic anisotropy energy, the small difference evaluated between these two parameters is also in favor of the existence of broad domain walls. Besides that, Figure 10b shows a similar plot from dc data, and the fit of the

dx.doi.org/10.1021/ic2020995 | Inorg. Chem. 2012, 51, 2885−2892

linear regime ($\mu_0 H_{DC}$ = 50 mT) affords values consistent with those from ac measurements.

Few other comments may be made from the plots of Figure 10; the first such logarithmic representation of χT versus T^{-1} shows linear behavior related to the Ising-like character of the magnetic chains in I^1O^2-CoC_{10}. However, deviations from this regime are observed at high and low temperature because of dominant intrachain antiferromagnetic coupling and LRO, respectively. More precisely, while the χT product saturates in some 1D systems at low temperature due to finite size effects,[32] here a marked decrease is observed for $\mu_0 H_{DC}$ = 0 T (Figure 10a), and χT strongly depends on the strength of the external field (Figure 10b). Neither the χT decrease in zero-field nor the strong field dependence of χT can be explained by a 1D model,[9] in agreement with the LRO found below T_t = 5.4 K. Second, we should point out that the temperature where χT starts to deviate from its exponential increase upon cooling down is largely affected by the applied magnetic field (Figure 10b). This behavior differs significantly from that reported in compounds such as the antiferromagnetic phase of $Mn^{III}_2Ni^{II}$ SCMs[9] where the variation of the χT product is field-dependent but where the temperature for which the χT product moves away from its exponential regime remains almost field-independent.

Magnetocaloric Properties. The magnetocaloric effect (MCE) of I^1O^2-CoC_{10} was evaluated from the C_P data shown in Figure 6a. The MCE corresponds to the adiabatic temperature change or the magnetic entropy change of a magnetic solid in a varying magnetic field.[33] Besides its possible use in applications such as adiabatic demagnetization refrigerators,[34] the MCE can also serve as a tool for investigating basic aspects of a magnetic material.[33] The isothermal magnetic entropy change $-\Delta S_M$ (Figure 11a) and adiabatic temperature change ΔT_{ad} (Figure 11b) were calculated from the measured heat capacity in various magnetic fields as described in ref 35. The total entropy of a magnetic solid in a given field can be calculated from the heat capacity as

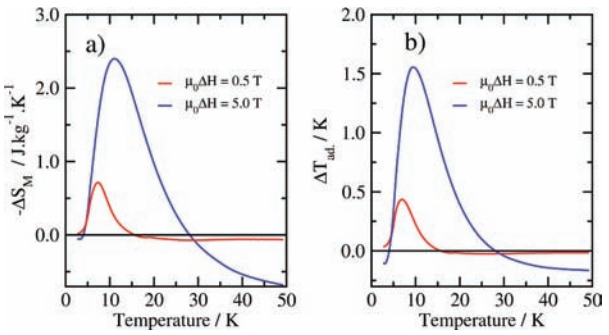

Figure 11. Temperature dependence of the MCE in I^1O^2-CoC_{10} for field variations of 0.5 and 5 T. (a) Magnetic entropy change. (b) Adiabatic temperature change.

$$S(T) = \int_0^T \frac{C_P(T)}{T}\,dT + S_0$$

where S_0 is the zero-temperature entropy. When integrating heat capacity data, the missing entropy below 2.5 K (the lowest temperature of the experiment) was taken into account by considering the linear variation of C_P down to 0 K. $\Delta S_M(T)$ is given by the isothermal difference (for a field variation $\Delta H = H_f - H_i$) between the $S(T)_{Hi}$ and $S(T)_{Hf}$ functions:

$$\Delta S_M(T)_{\Delta H} = [S(T)_{H_f} - S(T)_{H_i}]_T$$

while $\Delta T_{ad}(T)$ is calculated as their isentropic difference:

$$\Delta T_{ad}(T)_{\Delta H} = [T(S)_{H_f} - T(S)_{H_i}]_S$$

Upon field variation increase, the MCE peak due to the LRO transition at T_t broadens, shifts to higher temperatures, and increases in height, as expected for a second-order transition toward a magnetized state. The magnitude of the MCE associated with the LRO is quite moderate ($-\Delta S_M$ = 2.4 J kg^{-1} K^{-1} and ΔT_{ad} = 1.5 K for $\mu_0\Delta H$ = 5 T), about 10 times lower than that observed in the best magnetic refrigerants in the T range below 10 K such as, for instance, some *paramagnetic-like* molecular nanomagnets[36] or some intermetallic compounds with low ordering temperature.[33,37]

Above the LRO peak, the MCE changes sign since the applied field then competes with the antiferromagnetic intrachain interactions.[38] This very modest inverse magnetocaloric effect persists at temperatures well above T_t indicating that short-range correlations along the chains are present up to high temperatures.

CONCLUSIONS

In conclusion, our investigations into the chemistry of metal–organic frameworks, involving alkane dioic acids and transition metal elements in basic media, have afforded a structurally original compound with large interchain distances between "dense" magnetic chains. A detailed magnetic study of this compound was done and shows the coexistence of magnetic ordering and slow magnetic relaxation. The slow dynamical process occurring in the 3D ordered phase presumably originates from the strong 1D character of the magnetism (motion of broad domain walls) because of the weakness of the interchain interactions in comparison with intrachain one. The direct measurement of the LRO for such a metal–organic compound with 1D magnetic subnetwork is quite scarce in the literature. Our use of the heat capacity data for the calculation of the MCE has shown that it changes sign upon varying temperature, thus nicely illustrating the dimensional crossover between extended 1D correlation (SRO) and LRO.

We are currently working on the determination of the magnetic properties of I^1O^2-CoC_{10} at very low temperature as well as its magnetic structure as a function of temperature and applied magnetic field by high-flux neutron diffraction experiments. In a future report, a particular emphasis will be put on the signification of the high-temperature field-dependent ac peak described in this paper.

ASSOCIATED CONTENT

Supporting Information

Additional magnetic measurements, TGA, PXRD, and IR characterizations, as well as the CIF file of I^1O^2-CoC_{10}. This material is available free of charge via the Internet at http://pubs.acs.org.

AUTHOR INFORMATION

Corresponding Author

*E-mail: romain.sibille@ijl.nancy-universite.fr.

Notes

The authors declare no competing financial interest.

dx.doi.org/10.1021/ic2020995 | *Inorg. Chem.* 2012, 51, 2885–2892

■ ACKNOWLEDGMENTS

We are indebted to the Institut Laue Langevin (Grenoble, France) for the provision of research facilities, and our local contact (Silvia Capelli) is warmly acknowledged for her help during the recording of the patterns. We thank Lionel Aranda (Institut Jean Lamour, Nancy) for TG measurements. Pr. Davide M. Proserpio (University of Milan, Italy) is acknowledged for his help for the topological analysis. The authors are very grateful to Elsa Lhotel and Virginie Simonet (Institut Néel, Grenoble, France) for fruitful discussions.

■ REFERENCES

(1) (a) Tranchemontagne, D. J.; Mendoz-Cortes, J. L.; O'Keeffe, M.; Yaghi, O. M. *Chem. Soc. Rev.* **2009**, *38*, 1257−1283. (b) Horike, S.; Shimomura, S.; Kitagawa, S. *Nat. Chem.* **2009**, *1*, 695−704. (c) Ferey, G. *Chem. Soc. Rev.* **2008**, *37*, 191−214.

(2) (a) Weng, D. F.; Wang, Z. M.; Gao, S. *Chem. Soc. Rev.* **2011**, *40*, 3157−3181. (b) Dechambenoit, P.; Long, J. R. *Chem. Soc. Rev.* **2011**, *40*, 3249−3265. (c) Miller, J. S. *Chem. Soc. Rev.* **2011**, *40*, 3266−3296.

(3) (a) Kurmoo, M. *Chem. Soc. Rev.* **2009**, *38*, 1353−1379. (b) Huang, Z. L.; Drillon, M.; Masciocchi, N.; Sironi, A.; Zhao, J. T.; Rabu, P.; Panissod, P. *Chem. Mater.* **2000**, *12*, 2805−2812.

(4) (a) Cheetham, A. K.; Rao, C. N. R.; Feller, R. K. *Chem. Commun.* **2006**, 4780−4795. (b) Rao, C. N. R.; Cheetham, A. K.; Thirumurugan, A. *J. Phys.: Condens. Matter* **2008**, *20*, 083202.

(5) (a) Rueff, J. M.; Masciocchi, N.; Rabu, P.; Sironi, A.; Skoulios, A. *Chem.—Eur. J.* **2002**, *8*, 1813−1820. (b) Guillou, N.; Livage, C.; Férey, G. *Eur. J. Inorg. Chem.* **2006**, *24*, 4963−4978.

(6) Mesbah, A.; Carton, A.; Aranda, L.; Mazet, T.; Porcher, F.; François, M. *J. Solid State Chem.* **2008**, *181*, 3229−3235.

(7) Glauber, R. J. *J. Math. Phys.* **1963**, *4*, 294.

(8) Caneschi, A.; Gatteschi, D.; Lalioti, N.; Sangregorio, C.; Sessoli, R.; Venturi, G.; Vindigni, A.; Rettori, A.; Pini, M. G.; Novak, M. A. *Angew. Chem., Int. Ed.* **2001**, *40*, 1760−1763.

(9) Coulon, C.; Clérac, R.; Wernsdorfer, W.; Colin, T.; Miyasaka, H. *Phys. Rev. Lett.* **2009**, *102*, 167204.

(10) Miyasaka, H.; Takayama, K.; Saitoh, A.; Furukawa, S.; Yamashita, M.; Clérac, R. *Chem.—Eur. J.* **2010**, *16*, 3656−3662.

(11) Zhang, X. M.; Wang, Y. Q.; Wang, K.; Gao, E. Q.; Liu, C. M. *Chem. Commun.* **2011**, *47*, 1815−1817.

(12) (a) Minguet, M.; Luneau, D.; Lhotel, E.; Villar, V.; Paulsen, C.; Amabilino, D. B.; Veciana, J. *Angew. Chem., Int. Ed.* **2002**, *41*, 586−589. (b) Lhotel, E.; Simonet, V.; Ressouche, E.; Canals, B.; Amabilino, D. B.; Sporer, C.; Luneau, D.; Veciana, J.; Paulsen, C. *Phys. Rev. B* **2007**, *75*, 104429.

(13) (a) Baranov, N. V.; Mushnikov, N. V.; Goto, T.; Hosokoshi, Y.; Inoue, K. *J. Phys.: Condens. Matter* **2003**, *15*, 8881−8897. (b) Numata, Y.; Inoue, K.; Baranov, N. V.; Kurmoo, M.; Kikuchi, K. *J. Am. Chem. Soc.* **2007**, *129*, 9902−9909. (c) Bukharov, A. A.; Ovchinnikov, A. S.; Baranov, N. V.; Inoue, K. *J. Phys.: Condens. Matter* **2010**, *22*, 436003−436011.

(14) Ishii, N.; Okamura, Y.; Chiba, S.; Nogami, T.; Ishida, T. *J. Am. Chem. Soc.* **2008**, *130*, 24−25.

(15) Ovchinnikov, A. S.; Bostrem, I. G.; Sinitsyn, V. E.; Boyarchenkov, A. S.; Baranov., N. V.; Inoue, K. *Phys. Rev. B.* **2006**, *74*, 174427.

(16) Sessoli, R. *Angew. Chem., Int. Ed.* **2008**, *47*, 5508−5510.

(17) Favre-Nicolin, V.; Cerny, R. *J. Appl. Crystallogr.* **2002**, *35*, 734−743.

(18) Altomare, A.; Burla, M. C.; Camalli, G.; Cascarano, G.; Giacovazzo, C.; Gualiardi, A.; Polidori, G. *J. Appl. Crystallogr.* **1994**, *27*, 435.

(19) Sheldrick, G. M. *Acta Crystallogr., Sect. A* **2008**, *64*, 112−122.

(20) (a) Panissod, P.; Drillon, M. In *Magnetism: Molecules to Materials, IV*; Miller, J. S., Drillon, M., Eds.; Wiley-VCH: Weinheim, 2002; pp 233−270. (b) Wynn, C. M.; Gîrtu, M. A.; Brinckerhoff, W. B.; Sugiura, K. I.; Miller, J. S.; Epstein, A. J. *Chem. Mater.* **1997**, *9*, 2156−2163. (c) Ostrovsky, S.; Haase, W.; Drillon, M.; Panissod, P. *Phys. Rev. B* **2001**, *64*, 134418.

(21) The topological analysis has been done by using the TOPOS 4.0 program: Blatov, V. A. *IUCr CompComm. Newsletter* **2006**, *7*, 4−38.

(22) Kahn, O. *Molecular Magnetism*; VCH: New York, 1993.

(23) (a) Drillon, M.; Panissod, P.; Rabu, P.; Souletie, J.; Ksenofontov, V.; Gütlich, P. *Phys. Rev. B* **2002**, *65*, 104404. (b) Souletie, J.; Rabu, P.; Drillon, M. *Phys. Rev. B* **2005**, *72*, 214427. (c) Souletie, J.; Rabu, P.; Drillon, M. In *Magnetism: Molecules to Materials, V*; Miller, J. S., Drillon, M., Eds.; Wiley-VCH: Weinheim, 2005; pp 347−377.

(24) Zheng, Y. Z.; Xue, W.; Zhang, W. X.; Tong, M. L.; Chen, X. M.; Grandjean, F.; Long, G. L.; Ng, S. W.; Panissod, P.; Drillon, M. *Inorg. Chem.* **2009**, *48*, 2028−2042.

(25) Sengupta, P.; Sandvik, A. W.; Singh, R. R. P. *Phys. Rev. B* **2003**, *68*, 094423.

(26) (a) Lukin, J. A.; Friedberg, S. A.; DeFotis, G. C. *J. Appl. Phys.* **1991**, *69*, 5807. (b) Belik, A. A.; Azuma, M.; Takano, M. *Inorg. Chem.* **2003**, *42*, 8572.

(27) Coulon, C.; Miyasaka, H.; Clérac, R. *Struct. Bonding (Berlin)* **2006**, *122*, 163−206.

(28) Mydosh, J. A. *Spin Glasses: An Experimental Introduction*; Taylor & Francis: London, 1993.

(29) Hagiwara, M. *J. Magn. Magn. Mater.* **1998**, *89*, 177−181.

(30) Bogani, L.; Caneschi, A.; Fedi, M.; Gatteschi, M.; Massi, M.; Novak, M. A.; Pini, M. G.; Rettori, A.; Sessoli, R.; Vindigni, A. *Phys. Rev. Lett.* **2004**, *92*, 207204.

(31) Bogani, L.; Sessoli, R.; Pini, M. G.; Rettori, A.; Novak, M. A.; Rosa, P.; Massi, M.; Fedi, M.; Giuntini, L.; Caneschi, A.; Gatteschi, M. *Phys. Rev. B* **2005**, *72*, 064406.

(32) Coulon, C.; Clérac, R.; Lecren, L.; Wernsdorfer, W.; Miyasaka, H. *Phys. Rev. B* **2001**, *64*, 132408.

(33) Tishin, A. M.; Spichkin, Y. I. *The Magnetocaloric Effect and Its Applications*; IOP Publishing: Bristol, U.K., 2003.

(34) Shiron, P. J. *J. Low Temp. Phys.* **2007**, *148*, 915.

(35) Pecharsky, V. K.; Gschneidner, K. A. Jr. *J. Appl. Phys.* **1999**, *86*, 565−575.

(36) Evangelisti, M.; Brechin, E. K. *Dalton Trans.* **2010**, *39*, 4672−4676 and references therein.

(37) Pecharsky, V. K.; Gschneidner, K. A. Jr.; Toskol, A. O. *Rep. Prog. Phys.* **2005**, *68*, 1479−1539 and references therein.

(38) Sznajd, J. *Phys. Rev. B* **2008**, *78*, 214411.